Swampland criteria for a dark energy dominated universe ensuing from Gaussian processes and $H(z)$ data analysis

Emilio Elizalde[1,2,3,*] and Martiros Khurshudyan[1,2,3,4,5,†]

[1]*Consejo Superior de Investigaciones Científicas, ICE/CSIC-IEEC, Campus UAB, Carrer de Can Magrans s/n, 08193 Bellaterra (Barcelona) Spain*
[2]*International Laboratory for Theoretical Cosmology, Tomsk State University of Control Systems and Radioelectronics (TUSUR), 634050 Tomsk, Russia*
[3]*Research Division, Tomsk State Pedagogical University, 634061 Tomsk, Russia*
[4]*CAS Key Laboratory for Research in Galaxies and Cosmology, Department of Astronomy, University of Science and Technology of China, Hefei 230026, China*
[5]*School of Astronomy and Space Science, University of Science and Technology of China, Hefei 230026, China*

(Received 27 November 2018; published 29 May 2019)

Implications of string swampland criteria for a dark energy dominated universe, obtained through the use of Gaussian processes and $H(z)$ data analysis, are discussed, in particular, swampland criteria for a scalar-field dark energy without assuming any specific form for the potential. Allowing the Gaussian process to reconstruct the form of the potential from $H(z)$ data, upper bounds on the second swampland criterion ($SC2$, involving $|V'|/V$) for two different kernel functions [square exponential and Matern ($\nu = 9/2$) kernels] are estimated. The approach here differs from all previous studies, since the upper bound of the second Swampland criterion is derived in a thoroughly model-independent way, without employing a model-to-model comparison strategy. The analysis is performed using the latest values of H_0 reported by the Planck and Hubble missions. Results for the estimation of the constant of $SC2$ hint towards the possibility of getting upper bounds well behind the estimations for the dark energy dominated universe reported in previous studies, corresponding to the model-to-model comparison method. The estimation performed using the model-independent approach (Gaussian processes) turns out to be quite sensitive and dependent upon the data and kernel employed. This study is a first attempt towards the exploitation of the swampland criteria in a model-independent way and may be extended by involving other data sets and trying to understand what is the impact of higher-redshift data on the upper bounds. In the analysis, 40-point $H(z)$ data have been used, consisting of a 30-point sample deduced from a differential age method and an additional 10-point sample obtained from the radial BAO method. Hints towards the possibility of eventually disproving the swampland conjecture are noted.

DOI: 10.1103/PhysRevD.99.103533

I. INTRODUCTION

The accelerated expansion of the Universe [1–10] is a very surprising fact, which has been proven through several independent observations and is still open to different physical interpretations in terms of various gravity theories. In particular, the idea itself of dark energy, introduced in general relativity (GR) to address the physics of this phenomenon [11–22] (and references therein), acquires different forms. The first, and most simple, mathematical model for dark energy is the cosmological constant associated to the vacuum energy of the quantum fields at the cosmological level, giving origin to the cold dark matter model with cosmological constant Λ (ΛCDM), the standard cosmological model [23]. But, additionally, this simple model exhibits a theoretical problem, known as the cosmological coincidence problem [24,25]. This issue is the hidden motivation behind different dynamical and interacting dark energy models considered in the recent literature (see [11–22] and references therein). One of the possibilities, when we describe the background dynamics using GR, is to represent the dynamical dark energy by a scalar field. The usual way to obtain a model for the Universe having positive vacuum energy and involving a scalar field is to use a field potential with a local minimum at a positive value, leading to a stable or metastable de Sitter (dS) vacuum. Another interesting situation should be mentioned, too, namely, the case of quintessence models where the potential is positive but the scalar field is not at a minimum. This could occur when $|\nabla V|$ is sufficiently small and of the order of V itself.

*elizalde@ieec.uab.es
†khurshudyan@yandex.ru, khurshudyan@tusur.ru

On the other hand, according to the most common viewpoint, GR can in no way be the ultimate theory of the Universe, operating from cosmological scales to extremely small scales. Quantum corrections are bound to become important, and this is reflected in various viable modified theories of gravity that effectively deal with dark energy, dark matter, inflation, and other relevant problems [26–31] (to mention a few). We can however assume that GR might be the low-energy limit of a well-motivated (but yet to be found) high-energy UV-complete theory. In other words, we may play with the idea that the effective field theory has been originated from its low-energy limit and effectively captures the behavior of the inflaton field and dark energy phenomena. In this regard, string theory, which has the capacity to unify the standard model of particle physics with gravity, perfectly qualifies as a candidate for such an UV-complete theory.

However, an interesting situation has been met in string theory when confronted with the task of constructing dS vacua. Despite heroic attempts, until now no dS vacuum could be obtained, owing to numerous problems [32–54]. Therefore, we are led to assume, as of now, that in a consistent quantum theory of gravity, dS does not exist. The landscape provided by string theory yields the existence of a vast range of choices fitting our Universe in a consistent quantum theory of gravity; in other words, a whole landscape of vacua provided by string theory, which are believed to lead to consistent, effective field theories (EFT). However, taking into account the aforementioned problem with dS vacua, and that in the string landscape it is actually easy to obtain Minkowski and anti–de Sitter solutions, one is led to believe in the existence of the swampland—a region wherein inconsistent semiclassical EFTs inhabit. This statement can be understood as a claim of the existence of a set of consistently looking effective quantum field theories coupled to gravity, which are actually inconsistent with a quantum theory of gravity. And this could be an indicator that dS vacua may reside in the swampland [55,56].

In this promising context, it becomes an urgent task to investigate the cosmological implications of two of the proposed swampland criteria, expressed as

(1) $SC1$: the scalar field net excursion in reduced Planck units should satisfy the bound [55]

$$\frac{|\Delta\phi|}{M_P} < \Delta \sim O(1), \tag{1}$$

(2) $SC2$: the gradient of the scalar field potential is bounded by [56]

$$M_P \frac{|V'|}{V} > c \sim O(1), \tag{2}$$

if we consider GR with the standard matter fields in the presence of a quintessence field ϕ to be the effective field theory. Here, both Δ and c are positive constants of order one; the prime denotes the derivative with respect to the scalar field ϕ, and $M_P = 1/\sqrt{8\pi G}$ is the reduced Planck mass. On the other hand, it is well-known that this effective field theory admits solutions modeling an accelerated universe, and it is reasonable to investigate and try to understand what are the conditions to be satisfied in order not to end up in the swampland. In this regard, the one associated with the second swampland criterion ($SC2$), Eq. (2), is primarily relevant and the more interesting one to study. The two swampland criteria above demand that the field traverses a larger distance in order to have the domain of validity of the effective field theory and $SC2$ to be fulfilled.

An investigation of the implications of the string swampland criteria based on scalar field dark energy models [57] highlights the conditions to be met in order to remain outside of the swampland. Observational implications of future surveys on quintessence models with $V(\phi) \sim e^{-\lambda\phi}$, which impose constraints on λ, are also discussed there. An interesting question has arisen: how tightly future surveys will be able to decide whether dark energy is a cosmological constant or not. A first analysis shows that with the data expected from Euclid, the λ parameter should have to fall below 0.3, leaving only room for very small deviations of quintessence from a cosmological constant. On the other hand, the estimation constraining $\lambda < 0.1$ shows that the necessary survey volume would need to grow by a factor of $\sim$400, as compared to that covered by the Euclid survey. Therefore, one should expect fundamental observational limitations to lowering λ to $\lambda < 0.1$ with near-future surveys.

Present analyses, such as the one in [57], which can be considered an extension of [58], are being performed by using a model-by-model comparison method, in order to obtain the constraints on λ and on the $SC2$ constant c. In particular, the standard eight-parameter Chevallier-Polarski-Linder (CPL) cosmology is taken as a fiducial model to fit data, and then quintessence dark energy cosmology has been chosen as the comparison model. Finally, the simplest exponential potential for the quintessence field has been considered. On the other hand, also with a model-by-model comparison method based on the belief that the Universe should be multifeature and informative, possibly the largest upper bound on the swampland constant c has been reported recently in [59]. In that paper, interacting quintessence is considered as the comparison model for dark energy, constraining an 18-parameter extension of the ΛCDM cosmology, in light of current observations. The 3σ upper bound on the swampland constant c, following from this analysis, is 1.94. Such a result would permit, for instance, an 11-dimensional M-theory with a double-exponential potential to be the string-theory model for dark energy. It is interesting that using Bayesian evidence as the model selection tool, the

author found that this 18-parameter multifeature cosmological model is very strongly preferred over the ΛCDM cosmology. For more details, in relation to the results on the bounds of c relevant to inflation, we refer the readers to [59].

Also in [59], the urgent necessity to clarify several important aspects concerning previous studies, which have reported different upper bounds on c, has been expressed. In our opinion, these differences clearly indicate that interacting dark energy models can lead to interesting deviations from the cases with no interaction. One finds in the literature examples that show how a specific form of interaction can affect the structure formation process or how it can give rise to an effective degree of freedom to solve the cosmological coincidence problem and how this can be incorporated to the recently announced 21-cm anomaly. Some studies point to the fact that the result for the Hubble parameter at $z = 2.34$, reported by the BOSS experiment, is also an indication of a certain interaction between dark energy and dark matter. Moreover, we have examples where this interaction, understood as an energy transfer between them, can affect the precise type and the formation of future finite-time singularities (see, e.g., [11–22], for more details). In light of the above mentioned facts, the results in Ref. [59] indicate that the interaction between dark energy and dark matter can indeed have a strong impact on the bounds of the $SC2$, Eq. (2), constant c. However, to convert this guess into a solid conclusion, a deeper investigation is required, involving different forms of linear and nonlinear, sign fixed and sign changing interactions, as the ones considered in the recent literature.

It should be stressed again that all results discussed above have been obtained in a model-dependent way, by performing a model-to-model comparison. It is an urgent task to understand the upper bounds on c in a dark-energy dominated universe that are from different observational data in a model-independent way. Will the results change substantially? Our goal in this paper is to give an answer to this key question. For our purposes, we will use Gaussian process techniques (GP) and $H(z)$ data. It is well-known that the GP is a powerful tool allowing us to reconstruct the behavior of a function (and its derivatives) directly from given data [60] (see also [61]). Moreover, studies carried out in the recent literature have shown that with the GP method, it is possible to reconstruct the behavior of the nongravitational interaction between dark energy and dark matter (among other results). It should be noted that model-independent GP techniques depend on the covariance function (kernel), and that the hyperparameters describing it can be estimated directly from observational data (see [60–70], to mention a few). Therefore, we do not consider any specific parametrization for, e.g., the interaction term between dark energy and dark matter, but we can reconstruct it from observational data directly, by using the cosmological equations. Of course, in this case, reconstruction is possible if the description of dark energy is assumed. In general, the reconstruction of a function that is interesting for our study, in the scope of a certain cosmological model, will be easy to implement if we use the $H(z)$ data. This is obvious, since all cosmological quantities, after some algebra, can be eventually expressed as functions of the Hubble parameter and its derivatives; all of which can be reconstructed directly from the $H(z)$ data. Therefore, we are able, in particular, to model the deceleration parameter at different redshifts directly from $H(z)$, by using GP, since

$$q = -1 + (1+z)\frac{H'}{H}, \tag{3}$$

where the prime means the derivative with respect to the redshift.

In the next section, we will consider the data to be employed in this study, describing also how we can make use of GPs to reconstruct and estimate the swampland c parameter in a model-independent way. We will demonstrate that, for the study of the problem in this fashion, we do not need to make any assumptions concerning the form of the scalar-field potential or dark-energy model, nor go through any model-to-model comparison as has been done until now, e.g., in [57–59]. We refer the readers to several interesting works concerning the swampland criteria for an inflating universe [71–78], and to a recently appeared discussion on the possible types of singularities for the swampland potential $V(\phi) \sim e^{-\lambda\phi}$, analyzed by means of the asymptotic splitting method [79]. On the other hand, we should mention some clarifying discussions of the swampland criteria in two papers that appeared recently, [80,81].

The paper is organized as follows. In Sec. II, we present the data to be used in our analysis, discussing the strategy to be followed. In Sec. III, we introduce our model and obtain the equations, written in an appropriate form, which allow us to see how the reconstructed behavior of the Hubble parameter and its derivatives up to a high order can be used for the study of the swampland criteria in a model-independent way by directly using observational data. In Sec. IV, we discuss the results obtained from the reconstruction of two types of kernel functions and three different values of the Hubble parameter at $z = 0$ in each case. One of the values of H_0 used in our analysis has been estimated with the GP method and using high-redshift data for $H(z)$, while the other two are taken to be the values recently reported by the Planck [9] and Hubble [10] missions. To finish, the conclusions and a final discussion can be found in Sec. V.

II. DATA AND GAUSSIAN PROCESSES

In order to make the discussions in Secs. III and IV more transparent for the readers, we devote the present one to

some crucial aspects related to GP. In particular, we concentrate our attention on some crucial aspects related to the GP method, providing a basic knowledge of it. Additionally, the references may serve to find more information on the topic, with some cosmological applications existing in the recent literature. To start, we recall that the Gaussian distribution corresponds to a random variable characterized by a mean value and a covariance. Similar to Gaussian distributions, GPs should be understood as distributions over functions, characterized by a mean function and a covariance matrix. In other words, when we reconstruct a function $f(x)$ at x, the GP creates a Gaussian random variable with a mean $\mu(x)$ and variance $\sigma(x)$. But it is important to note that the function obtained at x using the GP depends on that obtained at $x+dx$, both being related by a covariance function, namely the GP, which correlates the values of the resulting function at different points. Therefore, the key ingredient of a GP is the covariance function, which for a given set of observations can infer the relation between independent and dependent variables. A number of possible choices for the covariance function exist—squared exponential, polynomial, spline, etc., to mention a few. In our studies, as a first option for the covariance function, we chose the commonly used squared exponential function,

$$k(x,x')=\sigma_f^2\exp\left(-\frac{(x-x')^2}{2l^2}\right), \tag{4}$$

where σ_f and l are parameters known as hyperparameters. These parameters represent the length scales in the GP. The l parameter corresponds to the correlation length along which the successive $f(x)$ values are correlated, while to control the variation in $f(x)$ relative to the mean of the process, we need the σ_f parameter. Therefore, the covariance between output variables will be written as a function of the inputs. Another interesting issue to be mentioned is that the covariance is maximum for variables whose inputs are very close. We should mention also that the two hyperparameters of Eq. (4) characterize the smoothness of the function $k(x,x')$, and their values will be eventually determined by the training of the data (assuming the errors are Gaussian), using either a maximum likelihood procedure or an optimization algorithm, which leads to the reconstructed function of interest. The training of the data to determine the values of the hyperparameters is applicable to all kernels, which can be used without any restriction. We can see from Eq. (4) that the squared exponential function is infinitely differentiable, a useful property in the case of constructing higher-order derivatives. However, it cannot be used, for instance, to identify and study possible singularities in the future or past, based on the data used to do the reconstruction. In this regard, GPs have limited power and cannot be used to study all types of problems of modern cosmology. On the other hand, the main benefit of using the GP approach is the avoidance to assume a parametric form of the function representing the data, based on particular models that may or may not be reasonable representations of the true measurements.

We have already mentioned that we have at our disposal various options to choose the kernel function, since we do not have any other method to decide which is its preferred form. In this regard it makes sense, in principle, to pick up one that only depends on the distances between different data points, as in the case of the kernel given by Eq. (4). However, to be sure that the choice of the covariance function is not unduly affecting the model selection, we have the choice to perform the analysis using another covariance function. Moreover, the discussion of the results of the study presented in Sec. IV will demonstrate that, although the choice of the kernel may modify the values of the bounds on $SC2$, the final outcome based on this approach is not changed qualitatively. As a consequence, following the recommendations mentioned above, coming from other studies (see, for instance, [63]) and with the aim to reveal additional aspects concerning the application of GP methods in the estimation of upper bounds for $SC2$, Eq. (2), we will also use here the so-called Matern ($\nu=9/2$) covariance function,

$$\begin{aligned}k_M(x,x')=\sigma_f^2\exp\left(-\frac{3|x-x'|}{l}\right)\\ \times\left[1+\frac{3|x-x'|}{l}+\frac{27(x-x')}{7l^2}\right.\\ \left.+\frac{18|x-x'|^3}{7l^3}+\frac{27(x-x')^4}{35l^4}\right].\end{aligned} \tag{5}$$

This is a popular covariance function. In Ref. [63], the Matern ($\nu=9/2$) kernel, Eq. (5), was the preferred one, because it led to the most reliable results amongst all the covariance functions involved in the analysis. This means, in particular, for Ref. [63], that for the various cosmological models and many realizations of mock data sets considered there, the model derived using this kernel lied on average within the reconstructed $1-\sigma$ limits for approximately 68% of the redshift range and within the reconstructed $2-\sigma$ limits for 95% of the redshift range. Moreover, for a detailed analysis regarding the optimal choice of the covariance function in a GP, in cosmological applications, we refer the readers to Ref. [67].

In what follows, we will use the freely available package GaPP (Gaussian Processes in Python) developed by Seikel *et al.* In [60], the authors provide a very complete description of the method (see also [62–70], for additional explanatory references). This technique allows us to choose different covariance functions, including the Matern covariance function given by Eq. (5), while the squared exponential function, Eq. (4), is used in the code as the default option. The code is also very useful to combine different

TABLE I. $H(z)$ and its uncertainty σ_H in units of $\mathrm{km\,s^{-1}\,Mpc^{-1}}$. In the upper panel, 30 samples deduced from the differential age method. In the lower one, 10 samples obtained from the radial BAO method. The table is according to [62] (see also references therein, for details).

z	$H(z)$	σ_H	z	$H(z)$	σ_H
0.070	69	19.6	0.4783	80.9	9
0.090	69	12	0.480	97	62
0.120	68.6	26.2	0.593	104	13
0.170	83	8	0.680	92	8
0.179	75	4	0.781	105	12
0.199	75	5	0.875	125	17
0.200	72.9	29.6	0.880	90	40
0.270	77	14	0.900	117	23
0.280	88.8	36.6	1.037	154	20
0.352	83	14	1.300	168	17
0.3802	83	13.5	1.363	160	33.6
0.400	95	17	1.4307	177	18
0.4004	77	10.2	1.530	140	14
0.4247	87.1	11.1	1.750	202	40
0.44497	92.8	12.9	1.965	186.5	50.4
0.24	79.69	2.65	0.60	87.9	6.1
0.35	84.4	7	0.73	97.3	7.0
0.43	86.45	3.68	2.30	224	8
0.44	82.6	7.8	2.34	222	7
0.57	92.4	4.5	2.36	226	8

observational data sets, provided the proper relation between them is known. Below, we present the data set we used and some clarification about the accepted strategy for our study, concerning the Hubble parameter value at $z = 0$. In particular, we use 30-point samples of $H(z)$ coming from the differential age method. Then, we add 10-point samples obtained from the radial BAO method (see Table I). In the first case, as we can see from Table I, we have relatively good data up to $z = 2$. On the other hand, the added data points from the radial BAO method allow us to extend the data range up to $z = 2.4$ improving also low-redshift data. However, we can see that the data points listed in Table I do not include the value of the Hubble parameter at $z = 0$, i.e., the value of H_0. This value will play an important role in our study in what will be seen in Sec. III at the theoretical level and in Sec. IV during the discussion of the results. It should be noted that in our study we will consider three different values for H_0. Specifically, the two values of H_0 reported by the Planck mission and the Hubble space telescope, respectively, and, in addition, we will let the GP itself to estimate a third value for H_0, from the values of the $H(z)$ data points corresponding to the higher redshifts, listed in Table I.

Recently, a situation similar to the last case has been considered, in a study relying on a new dark energy

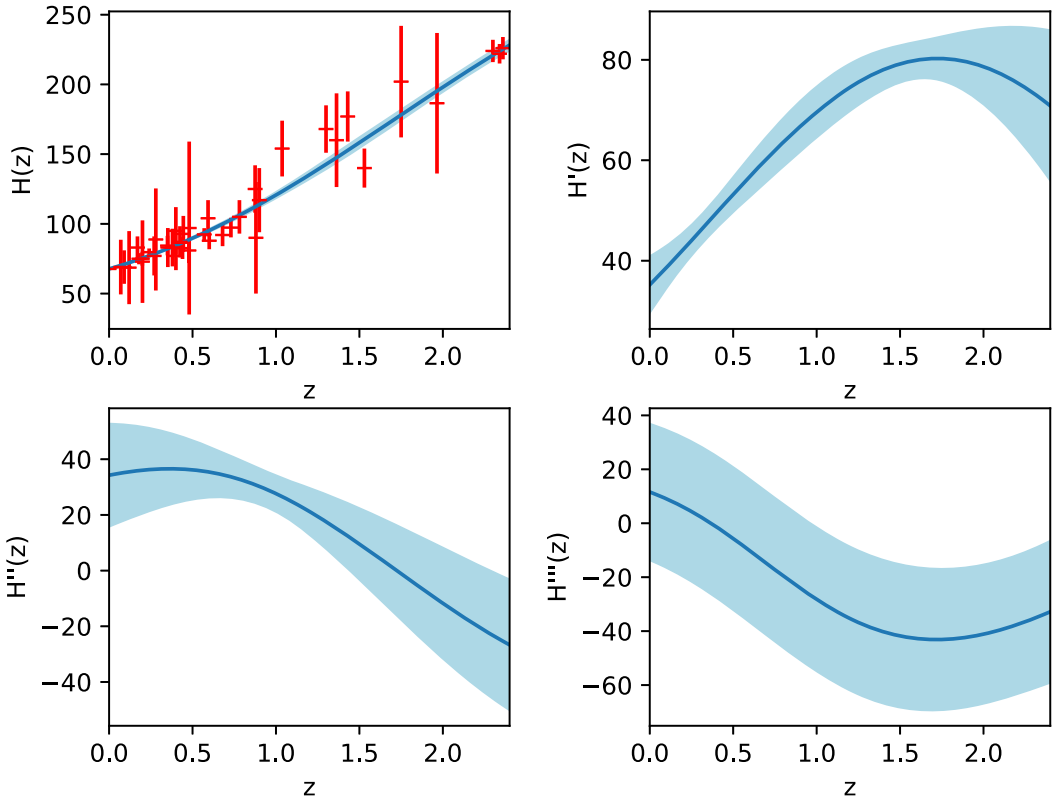

FIG. 1. GP reconstruction of $H(z)$, $H'(z)$, $H''(z)$, and $H'''(z)$, for the 40-point sample deduced from the differential age method, with an additional 10-point sample coming from the radial BAO method, for $H_0 = 67.66 \pm 0.42$ as reported by the Planck survey. Each prime means a derivative with respect to the redshift variable z.

parametrization, given by $\omega = \omega_0 + \omega_1 q$, where ω_0 and ω_1 are the parameters of the model to be determined and q is the deceleration parameter Eq. (3). To save space, let us refer the readers to [13], where the value of H_0 has been estimated for two cases using the GP directly. In particular, it was found in this reference that the GP can estimate the Hubble value for this case, yielding $H_0 = 71.286 \pm 3.743$ and 67.434 ± 4.748 (at 1σ reconstruction level) for 40 and 30-point samples of $H(z)$ data, respectively. On the other hand, in the same work, the authors discussed the reconstructed behavior of the Hubble parameter and its higher-order derivatives for the squared exponent kernel given by Eq. (4) [13]. Here, we present the results of the reconstruction for $H_0 = 67.66 \pm 0.42$ and $H_0 = 73.52 \pm 1.62$ reported from the Planck and Hubble surveys, respectively, for the Matern ($\nu = 9/2$) kernel, Eq. (5); see Figs. 1 and 2, which show the results of the reconstruction.

To end this section, note that a visual comparison of the behavior of the reconstructed H and $H'(z)$ reveals some differences between the two cases considered, described by the kernels given by Eqs. (4) and (5), respectively, which could induce some effect on the estimations under study. In the next section, we will see that, for this model-independent way of estimating the upper bound of $SC2$, we just need the reconstructed behavior of the Hubble parameter and its first-order derivative, when H_0 and Ω_{dm} at $z = 0$ are known. More on this issue in Sec. IV. On the other hand, since $SC2$ will be eventually expressed as a function of H and H', we can expect to obtain different upper bounds on $SC2$ for both cases. In the next section, we present a detailed demonstration of how the results of this one can be applied to the problem under study. Moreover, we should also mention a number of interesting papers where it is demonstrated that GPs can be used as an effective tool to select the best cosmological model among several acceptable possibilities [82–84].

III. THE MODEL

Here we shall consider GR with the standard matter field in the presence of a quintessence field ϕ to be the EFT described by the following action:

$$S = \int d^4x\sqrt{-g}\left(\frac{M_P^2}{2}R - \frac{1}{2}\partial_\mu\phi\partial^\mu\phi - V(\phi)\right) + S_m, \quad (6)$$

where S_m corresponds to standard matter, $M_P = 1/\sqrt{8\pi G}$ is the reduced Planck mass, R is the Ricci scalar, ϕ the field, and $V(\phi)$ is the field potential. It is well-known that, when we consider the Friedmann-Lemaître-Robertson-Walker universe, the dynamics of the scalar field's dark energy and dark matter are described by the equations,

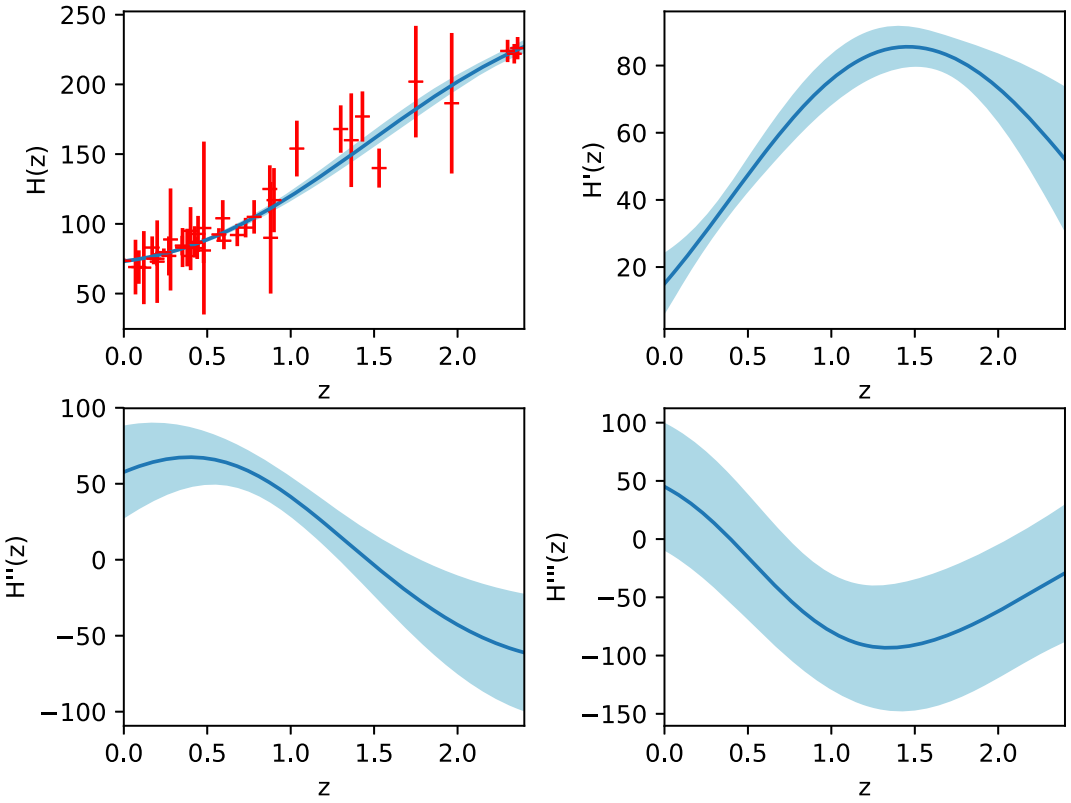

FIG. 2. GP reconstruction of $H(z)$, $H'(z)$, $H''(z)$, and $H'''(z)$ for the 40-point sample deduced from the differential age method, with an additional 10-point sample obtained from the radial BAO method, when $H_0 = 73.52 \pm 1.62$ as reported by the Hubble telescope. Each prime means the derivative with respect to the redshift z.

$$\dot{\rho}_\phi + 3H(\rho_\phi + P_\phi) = 0, \tag{7}$$

$$\dot{\rho}_{dm} + 3H\rho_{dm} = 0. \tag{8}$$

In other words, Eqs. (7) and (8) are the energy conservation laws for the components describing the background dynamics. Moreover, from the form of these equations, we see the absence of a coupling between the scalar field's dark energy and dark matter, which is accounted for in the recent literature as an energy flow between them. The presence of this coupling is interpreted as an interaction between dark energy and dark matter. Furthermore, we know that ρ_ϕ, ρ_{dm} and $P = P_\phi$ are related to each other through the Friedmann equations, as follows:

$$H^2 = \frac{1}{3}(\rho_\phi + \rho_{dm}), \tag{9}$$

and

$$\dot{H} + H = -\frac{1}{6}(\rho_\phi + \rho_{dm} + 3P_\phi). \tag{10}$$

If we now assume that the scalar field is spatially homogeneous, the corresponding energy density and pressure are

$$\rho_\phi = \frac{1}{2}\dot{\phi} + V(\phi), \tag{11}$$

and

$$P_\phi = \frac{1}{2}\dot{\phi} - V(\phi), \tag{12}$$

where the dot means the derivative with respect to the cosmic time, while $V(\phi)$ is the scalar field potential. In all the equations above, $H = \dot{a}/a$ is the Hubble parameter.

Now, we address some basic aspects concerning the background dynamics in the presence of scalar-field dark energy and standard matter: let us see how GPs can be involved in the study of such theories, in a model-independent way. In particular, how the $H(z)$ data obtained from astronomical observations can be used, bypassing the need to have the form of the scalar field potential be given in advance. From Eqs. (11) and (12), it is easy to see, in particular, that

$$\dot{\phi}^2 = \rho_\phi + P_\phi, \tag{13}$$

while

$$V(\phi) = \frac{\rho_\phi - P_\phi}{2}. \tag{14}$$

Now, from Eq. (8), we have $\rho_{dm} = 3H_0^2\Omega_0(1+z)^3$, then from Eq. (9), we can determine the energy density of the scalar field, which in the present case reads

$$\rho_\phi = 3H^2 - 3H_0^2\Omega_0(1+z)^3, \tag{15}$$

where H_0 is the Hubble parameter value at $z = 0$ (z is the redshift). It is then clear that in order to perform the analysis of the model and estimate the upper bound on $SC2$, we need to determine the functional dependence of P_ϕ on H. This is an easy task by using Eq. (10). After some algebra, we see that $P_\phi = 2(1+z)HH' - 3H^2$, where the prime denotes the derivative with respect to the redshift. Of course, we can see immediately that $\rho'_\phi = 6HH' - 9H_0^2\Omega_0(1+z)^2$ and $P'_\phi = 2(1+z)(H'^2 + HH'') - 4HH'$. Coming back to the form of $SC2$ to be reconstructed, we need only take into account that $dV(\phi)/d\phi = (dV/dz)/(d\phi/dz)$, where $d\phi/dz$ follows from Eq. (13) and that $\dot{\phi} = -(1+z)H\phi'$.

It is also easy to see that within the described approach, we are also able to reconstruct the equation of state (EoS) parameter of the model dark energy directly from the observational data. In particular, we can see that the EoS parameter is a function of the Hubble parameter and its first order derivative, specifically,

$$\omega_\phi = \frac{2(1+z)HH' - 3H^2}{3H^2 - 3H_0^2\Omega_0(1+z)^3}. \tag{16}$$

On the other hand, it is clear from Eq. (16), which allows us to reconstruct ω_ϕ from $H(z)$ data, that in order to estimate the upper bound on $SC2$ in a dark energy dominated universe, we can adopt another approach, different from the one used in this paper. In fact, we could reconstruct ω_ϕ from Eq. (16) and use it to obtain the constrains on the parameters present in the swampland potential. It is interesting to compare the results from different approaches to reconstruct the EoS parameter for dark energy (see, e.g., [85–87]). The results, from the GP reconstruction of ω_ϕ from the $H(z)$ data of Table I, are depicted in Fig. 3. The left panel corresponds to the GP reconstruction for the squared exponent kernel given by Eq. (4). For the right plot, the kernel is Matern ($\nu = 9/2$), given by Eq. (5). The solid line traces the mean of the reconstruction and the shaded blue regions are the 68% and 95% C.L. of the reconstruction, respectively. The value $H_0 = 67.66 \pm 0.42$ has been used, in accordance with the latest Planck results [9] with $M_P = 1$. Figure 3 points to the fact that during the GP reconstruction of ω_ϕ for the $H(z)$ data at higher redshifts, we are bound to observe very big reconstruction errors leading to rejection of the model. However, for low redshifts, when we have a dark energy dominated universe, GP reconstruction yields a well behaved mean and 68% and 95% C.L. strips of the reconstruction for ω_ϕ. The last one is the key aspect of our study, which allows us to estimate the upper bound on $SC2$ for each of the considered cases, because the behavior of ω_ϕ eventually determines the behavior of V'/V. In order to gain more knowledge on the subject under study, we

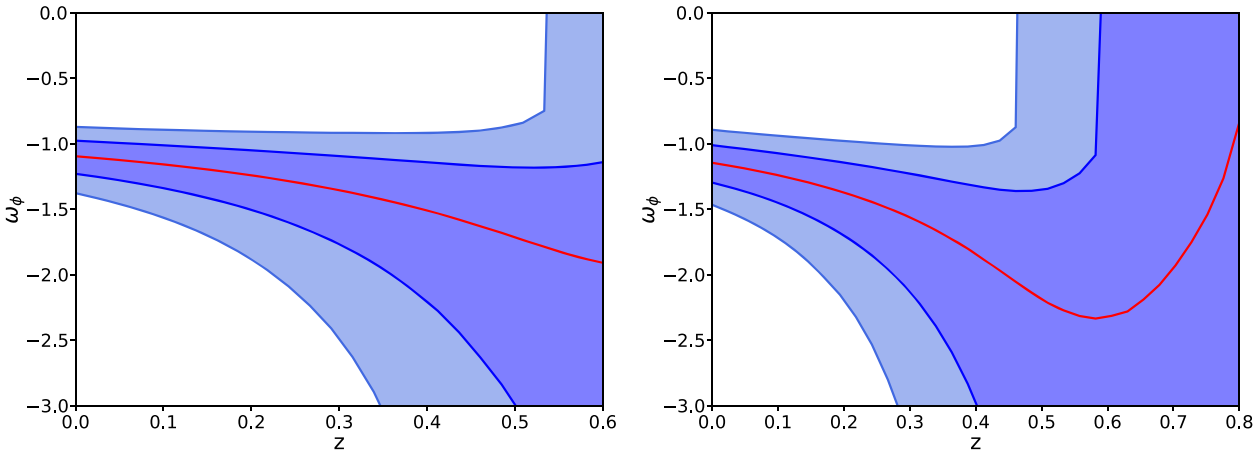

FIG. 3. Reconstruction of ω_ϕ, Eq. (16) from the $H(z)$ data in Table I. The left panel corresponds to GP reconstruction for the squared exponent kernel given by Eq. (4), while the right plot corresponds to the Matern $(\nu = 9/2)$, as a kernel, given by Eq. (5). The solid line depicts the mean of the reconstruction and the shaded blue regions are the 68% and 95% C.L. strips of the reconstruction, respectively. The value $H_0 = 67.66 \pm 0.42$ has been used, in accordance with the latest Planck results [9]. $M_P = 1$.

need to use data corresponding to higher redshifts and also deeper data sets. In this paper, however, we just concentrate our attention on $H(z)$ data and discuss some relevant consequences leaving these other important issues to subsequent study.

After all these considerations, it has become clear that we are in the position to reconstruct $SC2$ and to estimate its upper bound in a model-independent way, directly using observational data. The results of the study, for the strategies discussed in Sec. II, are presented in the next section.

IV. RESULTS

In Sec. II, we already mentioned that the analysis is carried out using two different kernel functions and for three different values of the Hubble parameter at $z = 0$. We start by presenting the results obtained for the first case, which corresponds to the squared-exponential kernel function, Eq. (4), while the value of the Hubble parameter comes from applying the GP to the higher-redshift data in Table I. In this case, we have seen that, according to the mean value of the reconstruction, $H_0 = 71.28$, while according to the 1σ reconstruction, the 1σ error is 3.74 [13]. On the other hand, the reconstruction of $\Omega_\phi = \rho_\phi/3H^2$ shows that the model should be rejected above $z = 1.9$ since the mean of the reconstruction predicts a negative Ω_ϕ. Moreover, we see also that, according to the reconstructed behavior of the mean, the dark energy dominated universe will be observed from $z = 0.27$, while according to the 2σ reconstruction band the dark energy dominated epoch will start from $z = 0.5$. On the other hand, we also have been able to estimate Ω_ϕ at $z = 0$ giving $\Omega_\phi = 0.7^{+0.05+0.08}_{-0.05-0.11}$ according to the mean, and 1σ and 2σ of the reconstruction bands, respectively.

It should be mentioned, as well, that the results obtained for 2σ could be questionable, since the estimation of Ω_ϕ from the reconstruction induces a tension, yielding results that are not consistent with those from other missions. However, for this case, we also estimated the upper bound on the constant c of $SC2$, Eq. (2). This could already be an indicator that we cannot trust too much the results from the reconstructed $SC2$, unless new data are available, for the low-redshift universe. The two plots of Fig. 4 correspond to the reconstruction of $SC2$ allowing us to estimate its upper bound, obtained by involving model-independent processes, as discussed above.

The left plot of Fig. 4 corresponds to the reconstruction of $SC2$ for the squared exponent case, Eq. (4), while the reconstruction corresponding to the Matern $(\nu = 9/2)$ kernel given by Eq. (5) can be found on the rhs plot. From these plots, we see, that the GP and $H(z)$ data presented in Table I yield a quite good reconstruction of $SC2$, allowing us to obtain the upper bounds on this parameter according to the mean, 1σ, and 2σ reconstructed bounds, respectively. The results of a further analysis show that:

(1) According to the mean of the reconstruction, in the case of the squared exponent kernel, Eq. (4), the dark energy dominated universe should start from $z = 0.27$, while we can observe a dark energy dominated universe from $z = 0.37$ according to the upper bound of the 1σ reconstruction. On the other hand, from $z = 0.5$, we can observe a dark energy dominated universe if we take into account the upper band from the 3σ reconstruction. The same picture has been observed after the reconstruction where we used the Matern $(\nu = 9/2)$ kernel given by Eq. (5). In addition, at $z = 0$, we will have $\omega_{\rm de} = -1.15$, $\omega_{\rm de} = -0.96$, and $\omega_{\rm de} = -0.76$, from the mean and the upper bounds for the 1σ and 2σ

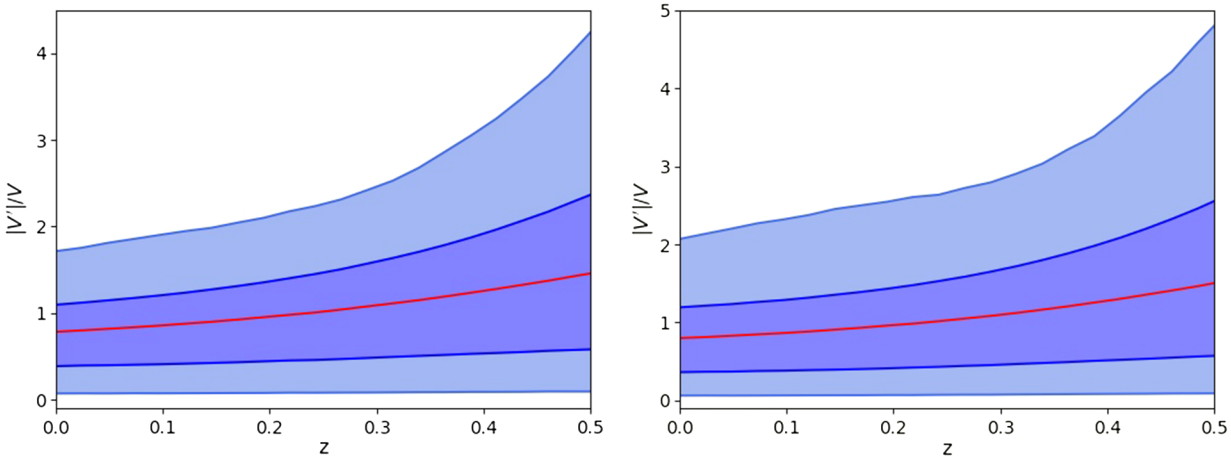

FIG. 4. Reconstruction of the $|V'|/V$, Eq. (2), from the $H(z)$ data depicted in Table I. The left panel represents GP reconstruction for the squared exponent kernel given by Eq. (4), while the right plot has been obtained considering the Matern $(\nu = 9/2)$ kernel given by Eq. (5). The solid line is the mean of the reconstruction and the shaded blue regions are the 68% and 95% C.L. of the reconstruction, respectively. $H_0 = 71.286 \pm 3.743$ has been estimated by GP using the data in Table I. $M_P = 1$.

reconstructions, respectively. However, when we start the estimation of $\omega_{\rm de}$ at $z = 0$, we observe that $\omega_{\rm de} = -1.13$, $\omega_{\rm de} = -0.93$, and $\omega_{\rm de} = -0.71$, from the mean and the upper bounds for the 1σ and 2σ reconstructions, respectively. Moreover, for this case, the following constraints for $\omega_{\rm de}$, Eq. (16): $\omega_{\rm de} = -1.15^{+0.19+0.39}_{-0.16-0.31}$ and $\omega_{\rm de} = -1.13^{+0.2+0.42}_{-0.18-0.33}$, have been obtained at $z = 0$ using the kernels given by Eqs. (4) and (5), respectively. It is obvious that according to the mean of the reconstruction, we should expect a phantom dark energy dominated universe at $z = 0$ in both cases. On the other hand, the upper bounds for the 1σ and 2σ reconstructions indicate the possibility to have a quintessence dark energy dominated universe. In contrast, according to the lower bounds for the 1σ and 2σ reconstructions, we should expect to observe the Universe being in a deep phantom dark energy dominated stage at $z = 0$. As a consequence, in this case, there is a tension with the constraints on $\omega_{\rm de}$ reported by PLANCK 2018 [9], which leaves room for additional analysis of the model involving high redshift data to be obtained soon from gravitational wave physics.

(2) On the other hand, according to the mean of the reconstruction, for the upper bound on the $SC2$ constant c for $z \in [0, 0.27]$, we will have 0.785. Moreover, according to the 1σ reconstruction, the upper bound on c for $z \in [0, 0.37]$ will be 1.786, while the 4.363 upper bound for c will be observed from the 3σ reconstruction bands. This estimation has been obtained with the squared exponent kernel, Eq. (4) (see the left plot of Fig. 4). When we use the Matern $(\nu = 9/2)$ kernel, Eq. (5), we observe that the upper bounds on c are 1.051, 1.886, and 4.926, respectively, as it has been discussed for the previous case (see the rhs plot in Fig. 4).

The results obtained from the case when we consider $H_0 = 73.52 \pm 1.62$ reported in [10] are summarized below and depicted in Fig. 5. In particular, we conclude that

(1) According to the mean of the reconstruction in the case of the squared exponent kernel, Eq. (4), the dark energy dominated universe starts at $z = 0.34$, while it will start at $z = 0.42$ according to the upper bound of the 1σ reconstruction. On the other hand, we will have a dark energy dominated universe starting at $z = 0.5$ if we take into account the upper band from the 3σ reconstruction. However, if the reconstruction is done by using the Matern $(\nu = 9/2)$ kernel of Eq. (5), then the dark energy dominated universe will be observed from $z = 0.27$, $z = 0.31$ and $z = 0.37$ for the mean and the upper bands of the 1σ and 2σ reconstruction, respectively. Moreover, at $z = 0$, we will have $\omega_{de} = -0.96$, $\omega_{de} = -0.88$, and $\omega_{de} = -0.81$ from the mean and from the upper bounds of the 1σ and 2σ reconstructions, respectively, when the kernel is given by Eq. (4). On the other hand, for the kernel given by Eq. (5), for the estimated value of ω_{de} at $z = 0$, we got $\omega_{de} = -1.23$, $\omega_{de} = -1.12$, and $\omega_{de} = -0.99$ from the mean and from the upper bounds of the 1σ and 2σ reconstructions, respectively. In addition, using the kernel given by Eq. (4), we get the following constraint on ω_{de}, Eq. (5): $\omega_{de} = -0.96^{+0.08+0.15}_{-0.09-0.16}$, while from the kernel given by Eq. (5), this other one follows: $\omega_{de} = -1.23^{+0.11+0.24}_{-0.12-0.23}$. The estimation of ω_{de} in this case reveals an interesting situation not observed in the previous one. Namely, we see that two different kernels predict two different states for the Universe at $z = 0$. In particular, the reconstruction with the kernel given by Eq. (4) predicts a quintessence universe for the mean and the upper bounds for the 1σ and 2σ reconstructions, respectively. However, according to the lower bound of the 1σ reconstruction,

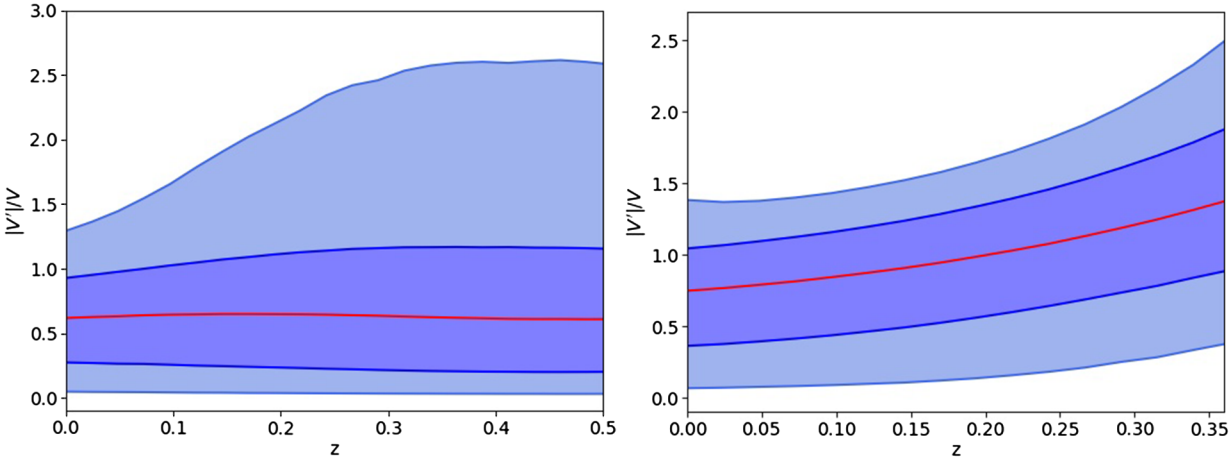

FIG. 5. Reconstruction of the $|V'|/V$, Eq. (2), from the $H(z)$ data in Table I. The left panel corresponds to the GP reconstruction for the squared exponent kernel given by Eq. (4), while the rhs plot has been obtained using the kernel to be Matern $(\nu = 9/2)$, Eq. (5). The solid line is the mean of the reconstruction, and the shaded blue regions are the 68% and 95% C.L. of the reconstruction, respectively. $H_0 = 73.52 \pm 1.62$ has been used according to the Hubble mission result [10]. $M_P = 1$.

in this case, we get a result in good agreement with the 2018 data reported from the PLANCK survey. Alternatively, if during the reconstruction, we use the kernel given by Eq. (5), then we obtain a phantom dark energy dominated universe, according to the mean of the reconstruction, while the upper bound of the 1σ reconstruction yields a value of ω_{de} at $z = 0$ in good agreement with the PLANCK 2018 results. In this regard, this particular case is more reliable than the one previously discussed.

(2) As for the upper bound on the $SC2$ constant c, again according to the mean of the reconstruction, for $z \in [0, 0.34]$, the bound is 0.649. And, according to the 1σ reconstruction, the upper bound on c for $z \in [0, 0.42]$ is 1.167, while 2.61 is the result obtained from the 3σ reconstruction bands on $z \in [0, 0.5]$. This has been obtained with the squared exponent kernel, Eq. (4) (see the left plot of Fig. 5). Alternatively, for the Matern $(\nu = 9/2)$ kernel, Eq. (5), we get the upper bounds on c to be 1.129, 1.691, and 2.52, respectively (see the right plot of Fig. 5), in the three corresponding cases.

Finally, we would like to summarize the results obtained from the study when we assume that the value of the Hubble parameter comes from the Planck survey result, i.e., $H_0 = 67.66 \pm 0.42$ [9]. The results for the two different kernel functions can be summarized as follows:

(1) According to the mean of the reconstruction, in the case of the squared exponent kernel, Eq. (4), the dark energy dominated universe starts at $z = 0.15$, while it does at $z = 0.25$, according to the upper bound of the 1σ reconstruction, and at $z = 0.36$, if we take into account the upper band from the 3σ reconstruction. However, if the reconstruction is done by using the Matern $(\nu = 9/2)$ kernel given by Eq. (5), then the dark energy dominated universe will be observed from $z = 0.09$, $z = 0.19$, and $z = 0.27$ for the mean and for the upper bands of the 1σ and 2σ reconstructions, respectively. Moreover, at $z = 0$, we will have $\omega_{\rm de} = -1.097$, $\omega_{\rm de} = -0.977$, and $\omega_{\rm de} = -0.872$ from the mean and from the upper bands of the 1σ and 2σ reconstructions, respectively, when the kernel is given by Eq. (4). On the other hand, when we consider the kernel given by Eq. (5), for the estimation of $\omega_{\rm de}$ at $z = 0$, we get $\omega_{\rm de} = -1.15$, $\omega_{\rm de} = -1.02$, and $\omega_{\rm de} = -0.89$, from the mean and from the upper bands corresponding to the 1σ and 2σ reconstructions, respectively. In this case, the following constraints at $z = 0$: $\omega_{\rm de} = -1.097^{+0.12+0.225}_{-0.133-0.28}$ and $\omega_{\rm de} = -1.15^{+0.13+0.26}_{-0.15-0.31}$, have been obtained as a result of the GP reconstruction for the kernels given by Eqs. (4) and (5), respectively. In other words, from the estimation of $\omega_{\rm de}$ and with proper 1σ and 2σ errors, the possibility to extract a value of $\omega_{\rm de}$ in a good agreement with the PLANCK 2018 results for ω_{de} is clear. This is also an interesting case indicating that future results obtained from this model can be trustable.

(2) As for the upper bound on the $SC2$ constant c for $z \in [0, 0.15]$, according to the mean of the reconstruction, we obtain 0.52. For the 1σ reconstruction, the upper bound on c for $z \in [0, 0.25]$ is 1.012, and the value increases considerably to 2.37 from the 3σ reconstruction bands on $z \in [0, 0.36]$. These estimations are obtained with the squared exponent kernel, Eq. (4) (left plot of Fig. 6). Finally, when we use the Matern $(\nu = 9/2)$ kernel, Eq. (5), the upper bounds on c are 0.51, 1.02, and 2.895, respectively (rhs plot of Fig. 6).

In summary, our analysis here has allowed us to estimate the upper bound on the constant of $SC2$ using a GP and 40-point $H(z)$ data. This is a fully model-independent

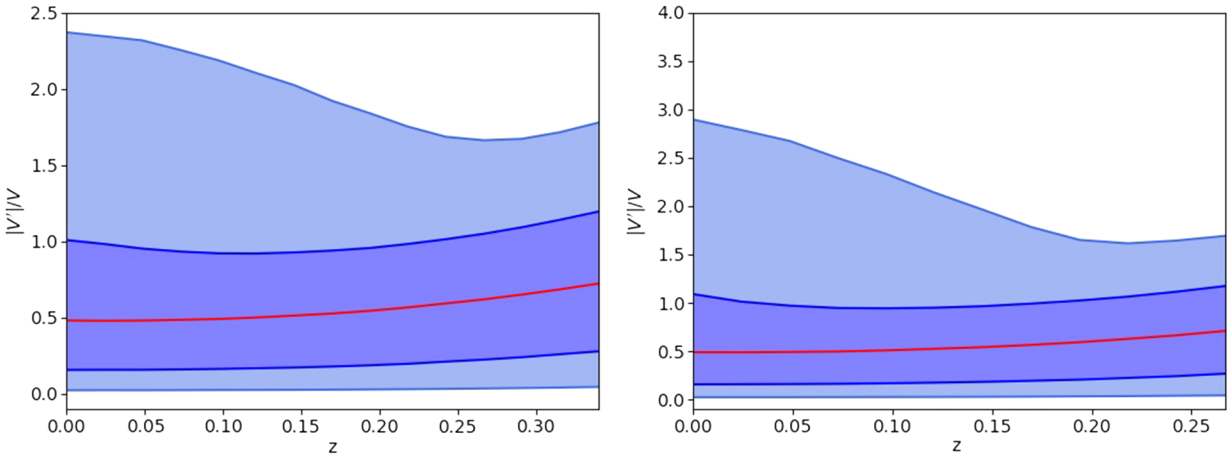

FIG. 6. Reconstruction of $|V'|/V$, Eq. (2), from the $H(z)$ data in Table I. The left panel corresponds to the GP reconstruction for the squared exponent kernel given by Eq. (4), while the right plot is for the Matern $(\nu = 9/2)$ kernel, Eq. (5). The solid line depicts the mean of the reconstruction and the shaded blue regions are the 68% and 95% C.L. bands of the reconstruction, respectively. The value $H_0 = 67.66 \pm 0.42$ has been used, in accordance with the latest Planck survey results [9]. $M_P = 1$.

estimation, since we do not make any assumption about the form of the swampland potential, neither assume any *a priori* model in order to do the estimation. According to the discussion presented above, we found that, when $H_0 = 67.66 \pm 0.42$, according to the Planck results, then the upper bounds on the $SC2$ constant are 2.37 and 2.895, for the squared exponent and Matern $(\nu = 9/2)$ kernel, respectively. On the other hand, when $H_0 = 73.52 \pm 1.62$, then the model-independent estimation of the upper bounds are found to be 1.167, according to the 1σ reconstruction. Alternatively, when we use the Matern $(\nu = 9/2)$ kernel, Eq. (5), the upper bound moves to 1.691. And, when $H_0 = 71.286 \pm 3.743$ is considered, the upper bound on $SC2$ is at 0.785. Furthermore, according to the 1σ reconstruction the upper bound on c reads 1.786 (for the squared kernel function). However, when we use the Matern $(\nu = 9/2)$ kernel, Eq. (5), then the upper bounds on c are 1.051 and 1.886, respectively.

The above estimations of the upper bound of the constant c of $SC2$, Eq. (2), prove the possibility to have different upper bounds depending on the kernel function considered, and on the precise, present value of the Hubble parameter. This is a very interesting result, which nontrivially complements the upper bounds reported by other (model-dependent) studies in the recent literature. In particular, our results are perfectly consistent with the results reported in [59]. But, on the other hand, we see that, in a model-independent analysis as the one performed here, we can even reach upper bounds behind these, what had been advanced as a feasible possibility in previous studies. Our results here clearly indicate that each detail concerning the way the fit is performed, the background dynamics in model-to-model comparison methods adopted in previous studies, including the priors and used data sets, can significantly affect the final values obtained for the upper bounds on c. Moreover, with the GP estimation of the upper bound on c adopted here, in order to reject or recover the status of EFT theories, one still requires additional analysis considering other data sets and kernels with different priors on the hyperparameters. The study here performed should be viewed as just a first (albeit already fruitful) attempt to use GP methods to study swampland criteria for the dark energy dominated universe. We have also imposed constraints on $\omega_{\rm de}$ in a model-independent way and proven that it is possible to obtain the present state of the Universe at $z = 0$ with a dark energy having an EoS parameter in good agreement with the PLANCK 2018 data run. Anyway, since constraining the EoS parameter for dark energy was not the preliminary goal of this paper, we leave a more detailed analysis of this issue and its comparison with other studies for future investigation.

V. DISCUSSION

In this paper, we have used GP techniques in order to investigate the implications of the string swampland criteria for a scalar-field dark-energy dominated universe, without assuming any prior specific form for the field potential. In other words, we have considered GR, with a standard matter field in the presence of a quintessence field, ϕ, without fixing the field potential, to be the effective field theory. Our study consists in a fully model-independent analysis: we invoke GP to reconstruct the form of the potential from $H(z)$ data and estimate at the same time the upper bound on the constant c of $SC2$. The 40-points $H(z)$ data used in the process consist of 30-point samples coming from the differential age method and additional 10-point samples obtained from the radial BAO method.

The upper bounds on the second swampland criteria $(|V'|/V)$ have been estimated both for the squared exponent

and Matern ($\nu = 9/2$) kernels, for three different values of H_0 in each case. Specifically, in one case, we have made use of the GP working with the $H(z)$ data sample to estimate the value of H_0, while in the other two situations, we have considered values of H_0 compatible with those reported by the Planck and Hubble missions, i.e., $H_0 = 67.66 \pm 0.42$, and $H_0 = 73.52 \pm 1.62$, respectively. After some algebra, we have found that in the absence of a coupling between the scalar field's dark energy and dark matter, we can express $SC2$, Eq. (2), in terms of H and H', which are reconstructed by means of the GP. After establishing a proper mathematical background, we were able to estimate the upper bounds on $SC2$, for each case, in a completely model-independent way. It is obvious that this approach is quite different from previous model-to-model comparisons; however, the estimations do heavily depend on the quality of the data used for the reconstruction. Eventually, estimations also rely on the kernel used, which not only controls the mean value of the reconstruction, but also the error bars of the same and the reconstruction of the derivatives of the H parameter as well. We should stress once more that previous estimations of the upper bounds on the constant of $SC2$ were based on methods involving model-to-model comparison, while here we have merely used a kernel and performed the estimation from the best observational data available.

In parallel to the reconstruction of $SC2$ and in order to estimate the upper bounds on its value, we have also reconstructed $\Omega_{\rm de}$, $\omega_{\rm de}$ and could estimate at which redshifts the dark energy dominated universe can be observed, in order to address the $SC2$ estimation. In particular, we have concluded that when we involve the GP alone to estimate the Hubble parameter value at $z = 0$ (found to be $H_0 = 71.286 \pm 3.743$), then according to the mean value of the reconstruction, in the case of the squared exponent kernel, the dark energy dominated universe starts at $z = 0.27$. On the other hand, the dark energy dominated universe will start at $z = 0.37$, when the upper bound of the 1σ reconstruction is used. Finally, in the case we take into account the upper band corresponding to the 3σ reconstruction, we get a dark-energy dominated universe from $z = 0.5$ onward.

A similar picture has been obtained as a result of the reconstruction procedure, when we have used the Matern ($\nu = 9/2$) kernel given by Eq. (5). The reconstruction of $\Omega_\phi = \rho_\phi/3H^2$ shows that the model should be rejected above $z = 1.9$, since the mean of the reconstruction predicts a negative Ω_ϕ. Eventually, we were also able to estimate Ω_ϕ at $z = 0$, yielding $\Omega_\phi = 0.7^{+0.05+0.08}_{-0.05-0.11}$, according to the mean and 1σ and 2σ results for the reconstruction bands, respectively. The above analysis yields the following results for the squared kernel function: according to the mean of the reconstruction, the upper bound on the $SC2$ is 0.785; for the 1σ reconstruction, the upper bound on c is 1.786, while for the 3σ reconstruction, we get 4.363 as upper bound for c. Alternatively, when we used the Matern ($\nu = 9/2$) kernel, Eq. (5), we obtained that the upper bounds on c turn out to be 1.051, 1.886, and 4.926, respectively. Surprisingly, in both situations, higher upper bounds have been obtained for the 3σ reconstruction bounds, in which case $\Omega_\phi = 0.782$, for both kernel functions. Therefore, the most reliable outcome, in the form of an upper bound for the c constant of $SC2$ appears to be 1.786 and 1.886, obtained from the 2σ reconstruction bounds for the two kernels, respectively.

In addition, considering $H_0 = 73.52 \pm 1.62$ and estimating Ω_ϕ at $z = 0$, we are led to $\Omega_\phi = 0.74$, for the upper bound of the 3σ reconstruction. Again, in this case, similarly to the first case discussed above, we better trust the results obtained from the mean and 1σ reconstruction bands. In this regard, according to the mean value of the reconstruction, the upper bound lies at 0.649, while it rises to 1.167, according to the 1σ reconstruction. Alternatively, when using the Matern ($\nu = 9/2$) kernel, Eq. (5), we observed that the upper bounds on c turn to be 1.129 and 1.691, for the mean and 2σ reconstruction bands, respectively.

Finally, the analysis of the case when $H_0 = 67.66 \pm 0.42$ has been performed. It reveals that, as more reliable upper bounds on the constant of $SC2$, those obtained from 1σ and 2σ reconstructions should be taken, because only for them can one obtain results for Ω_ϕ and ω_ϕ that are consistent with the results reported by other studies. In this case, for the upper bound for $SC2$, we get 1.012 and 2.37, when the squared exponent kernel is considered. If we start from the Matern ($\nu = 9/2$) kernel, the consistent background dynamics can be observed when using the 1σ and 2σ reconstruction upper bands, namely 1.02 and 2.895, respectively.

As argued above, the dS solution seems to be in the swampland, what would rule out ΛCDM in the future of the universe and maybe start to generate some tensions at present. More specifically, it has been argued in [88] that $H(z)$ ought to have a turning point at some low value of z, but the results of our analysis do not seem to show such implication. It appears as if, at the level of our present research, the swampland conjecture could be disproven. However, it would not be reasonable to adventure such a result with only one case considered; a more rigorous analysis using different data sets when involving the GP must be undertaken in order to be able to reach such a sharp and important conclusion. We expect to return to this relevant point soon, by increasing the accuracy of our analysis.

To summarize, our model-independent estimations for $SC2$ are in good agreement with the results reported in [59] for the dark energy dominated universe. However, we have noticed the possibility to get higher upper bounds on the $SC2$ constant, never reported before. This probably could be achieved directly, by using appropriate forms for the

interaction term between the scalar field and dark matter. This may be, of course, a hard task to perform, since there are various possible forms for the interaction term and checking any of them is a very time-consuming process. In this regard, using GP techniques can again be very useful. The study reported here indicates that every detail, concerning the way the fit was performed, and the background dynamics in the model-to-model comparison method adopted in previous studies, including the priors and data sets used, can significantly affect the results on the upper bounds of c. Within the adopted GP estimation method of the upper bound on c, in order to be able to either reject or recover the status of EFT theories, additional analysis is still required, starting with the consideration of other data sets and kernels with different priors for the hyperparameters. Our study, as reported here, is to be pondered as a first, albeit already revealing, attempt to show the benefits of using GP techniques in the study of swampland criteria for the dark-energy dominated universe.

ACKNOWLEDGMENTS

We thank Maurice van Putten for interesting comments. We thank also an anonymous referee for valuable and constructive suggestions to improve the structure and presentation of the paper. E. E. has been partially supported by MINECO (Spain), Project No. FIS2016-76363-P, by the Catalan Government 2017-SGR-247, and by the CPAN Consolider Ingenio 2010 Project. M. K. is supported in part by a CAS President's International Fellowship Initiative Grant No. 2018PM0054 and the NSFC (No. 11847226).

[1] A. G. Riess *et al.*, Astron. J. **116**, 1009 (1998).
[2] S. Perlmutter *et al.*, Astrophys. J. **517**, 565 (1999).
[3] Y. Sofue and V. Rubin, Annu. Rev. Astron. Astrophys. **39**, 137 (2001).
[4] M. Bartelmann and P. Schneider, Phys. Rep. **340**, 291 (2001).
[5] D. Clowe, A. Gonzalez, and M. Markevitch, Astrophys. J. **604**, 596 (2004).
[6] G. Hinshaw *et al.* (WMAP Collaboration), Astrophys. J. Suppl. Ser. **208**, 19 (2013).
[7] P. A. R. Ade *et al.* (Planck Collaboration), Astron. Astrophys. **571**, A16 (2014).
[8] P. A. R. Ade *et al.* (Planck Collaboration), Astron. Astrophys. **594**, A13 (2016).
[9] N. Aghanim *et al.* (Planck Collaboration), arXiv:1807.06209.
[10] A. G. Riess *et al.*, Astrophys. J. **861**, 126 (2018).
[11] J. Yoo and Y. Watanabe, Int. J. Mod. Phys. D **21**, 1230002 (2012).
[12] A. A. Costa, R. C. G. Landim, B. Wang, and E. Abdalla, Eur. Phys. J. C **78**, 746 (2018).
[13] E. Elizalde, M. Khurshudyan, and S. Nojiri, Int. J. Mod. Phys. D **28**, 1950019 (2019).
[14] E. Elizalde and M. Khurshudyan, Int. J. Mod. Phys. D **27**, 1850037 (2018).
[15] Y. L. Bolotin, A. Kostenko, O. A. Lemets, and D. A. Yerokhin, Int. J. Mod. Phys. D **24**, 1530007 (2015).
[16] M. Khurshudyan and R. Myrzakulov, Eur. Phys. J. C **77**, 65 (2017).
[17] M. Khurshudyan, Astrophys. Space Sci. **360**, 33 (2015).
[18] M. Khurshudyan and As. Khurshudyan, Symmetry **10**, 577 (2018).
[19] M. Khurshudyan, Eur. Phys. J. Plus **131**, 25 (2016).
[20] M. Khurshudyan, Mod. Phys. Lett. A **31**, 1650055 (2016).
[21] M. Khurshudyan, Mod. Phys. Lett. A **31**, 1650097 (2016).
[22] M. Khurshudyan, Symmetry **8**, 110 (2016).
[23] S. Weinberg, Rev. Mod. Phys. **61**, 1 (1989).
[24] H. E. S. Velten, R. F. vom Marttens, and W. Zimdahl, Eur. Phys. J. C **74**, 3160 (2014).
[25] N. Sivanandam, Phys. Rev. D **87**, 083514 (2013).
[26] S. Nojiri, S. D. Odintsov, and V. K. Oikonomou, Phys. Rep. **692**, 1 (2017).
[27] S. Nojiri and S. D. Odintsov, eConf **C0602061**, 115 (2006); Int. J. Geom. Methods Mod. Phys. **04**, 115 (2007).
[28] S. Nojiri and S. D. Odintsov, Phys. Rep. **505**, 59 (2011).
[29] E. Elizalde, S. Nojiri, S. D. Odintsov, and D. Saez-Gomez, Eur. Phys. J. C **70**, 351 (2010).
[30] E. Elizalde, R. Myrzakulov, V. V. Obukhov, and D. Saez-Gomez, Classical Quantum Gravity **27**, 095007 (2010).
[31] G. Cognola, E. Elizalde, S. Nojiri, S. D. Odintsov, L. Sebastiani, and S. Zerbini, Phys. Rev. D **77**, 046009 (2008).
[32] S. Kachru, R. Kallosh, A. D. Linde, and S. P. Trivedi, Phys. Rev. D **68**, 046005 (2003).
[33] V. Balasubramanian, P. Berglund, J. P. Conlon, and F. Quevedo, J. High Energy Phys. 03 (2005) 007.
[34] A. Westphal, J. High Energy Phys. 03 (2007) 102.
[35] X. Dong, B. Horn, E. Silverstein, and G. Torroba, Classical Quantum Gravity **27**, 245020 (2010).
[36] M. Rummel and A. Westphal, J. High Energy Phys. 01 (2012) 020.
[37] J. Blbck, U. Danielsson, and G. Dibitetto, J. Cosmol. Astropart. Phys. 03 (2014) 003.
[38] M. Cicoli, D. Klevers, S. Krippendorf, C. Mayrhofer, F. Quevedo, and R. Valandro, J. High Energy Phys. 05 (2014) 001.
[39] J. M. Maldacena and C. Nunez, Int. J. Mod. Phys. A **16**, 822 (2001).
[40] P. K. Townsend, arXiv:hep-th/0308149.
[41] M. P. Hertzberg, S. Kachru, W. Taylor, and M. Tegmark, J. High Energy Phys. 12 (2007) 095.
[42] C. Caviezel, T. Wrase, and M. Zagermann, J. High Energy Phys. 04 (2010) 011.

[43] B. de Carlos, A. Guarino, and J. M. Moreno, J. High Energy Phys. 01 (2010) 012.
[44] G. Shiu and Y. Sumitomo, J. High Energy Phys. 09 (2011) 052.
[45] S. R. Green, E. J. Martinec, C. Quigley, and S. Sethi, Classical Quantum Gravity **29**, 075006 (2012).
[46] F. F. Gautason, D. Junghans, and M. Zagermann, J. High Energy Phys. 06 (2012) 029.
[47] D. Kutasov, T. Maxfield, I. Melnikov, and S. Sethi, Phys. Rev. Lett. **115**, 071305 (2015).
[48] D. Junghans, J. High Energy Phys. 06 (2016) 132.
[49] D. Andriot and J. Blbck, J. High Energy Phys. 03 (2017) 102.
[50] D. Andriot, J. High Energy Phys. 03 (2018) 054.
[51] D. Andriot, Fortschr. Phys. **67**, 1800103 (2019).
[52] C. Han, S. Pi, and M. Sasaki, Phys. Lett. B **791**, 314 (2019).
[53] J. Moritz, A. Retolaza, and A. Westphal, Phys. Rev. D **97**, 046010 (2018).
[54] U. H. Danielsson and T. Van Riet, Int. J. Mod. Phys. D **27**, 1830007 (2018).
[55] H. Ooguri and C. Vafa, Nucl. Phys. **B766**, 21 (2007).
[56] G. Obied, H. Ooguri, L. Spodyneiko, and C. Vafa, arXiv: 1806.08362.
[57] L. Heisenberg, M. Bartelmann, R. Brandenberger, and A. Refregier, Phys. Rev. D **98**, 123502 (2018).
[58] P. Agrawal, G. Obied, P. J. Steinhardt, and C. Vafa, Phys. Lett. B **784**, 271 (2018).
[59] D. Wang, arXiv:1809.04854.
[60] M. Seikel, C. Clarkson, and M. Smith, J. Cosmol. Astropart. Phys. 06 (2012) 036.
[61] H. Yu, B. Ratra, and F.-Y. Wang, Astrophys. J. **856**, 3 (2018).
[62] M.-J. Zhang and J.-Q. Xia, J. Cosmol. Astropart. Phys. 12 (2016) 005.
[63] S. Yahya, M. Seikel, C. Clarkson, R. Maartens, and M. Smith, Phys. Rev. D **89**, 023503 (2014).
[64] R. G. Cai, N. Tamanini, and T. Yang, J. Cosmol. Astropart. Phys. 05 (2017) 031.
[65] R. G. Cai and T. Yang, Phys. Rev. D **95**, 044024 (2017).
[66] D. Wang and X.-H. Meng, Phys. Rev. D **95**, 023508 (2017).
[67] M. Seikel and C. Clarkson, arXiv:1311.6678.
[68] S. Santos-da Costa, V. C. Busti, and R. F. L. Holanda, J. Cosmol. Astropart. Phys. 10 (2015) 061.
[69] T. Holsclaw, U. Alam, B. Sansó, H. Lee, K. Heitmann, S. Habib, and D. Higdon, Phys. Rev. Lett. **105**, 241302 (2010).
[70] T. Yang, Z. K. Guo, and R. G. Cai, Phys. Rev. D **91**, 123533 (2015).
[71] S. Brahma and Md. Wali Hossain, J. High Energy Phys. 03 (2019) 006.
[72] K. Dimopoulos, Phys. Rev. D **98**, 123516 (2018).
[73] S. Das, Phys. Rev. D **99**, 063514 (2019).
[74] S. Das, Phys. Rev. D **99**, 083510 (2019).
[75] A. Ashoorioon, Phys. Lett. B **790**, 568 (2019).
[76] G. D'Amico, N. Kaloper, and A. Lawrence, arXiv:1809 .05109.
[77] W. H. Kinney, S. Vagnozzi, and L. Visinelli, Classical Quantum Gravity **36**, 117001 (2019).
[78] S. K. Garg and C. Krishnan, arXiv:1807.05193.
[79] S. D. Odintsov and V. K. Oikonomou, arXiv:1810.03575.
[80] L. Heisenberg *et al.*, Fortschr. Phys. **67**, 1800075 (2019).
[81] Y. Akrami, R. Kallosh, A. Linde, V. Vardanyan, Fortschr. Phys. **67**, 1800075 (2019).
[82] F. Melia and M. K. Yennapureddy, J. Cosmol. Astropart. Phys. 02 (2018) 034.
[83] M. K. Yennapureddy and F. Melia, Eur. Phys. J. C **78**, 258 (2018).
[84] M. K. Yennapureddy and F. Melia, J. Cosmol. Astropart. Phys. 11 (2017) 029.
[85] A. Mehrabi and S. Basilakos, Eur. Phys. J. C **78**, 889 (2018).
[86] J. A. Vazquez, M. Bridges, M. P. Hobson, and A. N. Lasenby, J. Cosmol. Astropart. Phys. 09 (2012) 020.
[87] T. Holsclaw, U. Alam, B. Sansó, H. Lee, K. Heitmann, S. Habib, and D. Higdon, Phys. Rev. Lett. **105**, 241302 (2010).
[88] E. O. Colgain, M. H. P. M. van Putten, and H. Yavartanoo, Phys. Lett. B **793**, 126 (2019).